Journal of the Australian Ceramic Society
https://doi.org/10.1007/s41779-025-01214-y

RESEARCH

Synthesis, characterization, and photocatalytic applications of ZnO nanoparticles-embedded PMMA nanocomposites for sustainable water purification

Hamoudi Belhoul[1,2] · Smail Terchi[1,2] · Naziha Ladjal[1,3] · Lamya Meftah[1,2] · Bahri Deghfel[1,4] · Abdelhalim Zoukel[5] · Ahmad Azmin Mohamad[6]

Received: 10 February 2025 / Revised: 7 May 2025 / Accepted: 9 May 2025

Abstract

This study involves the synthesis of zinc oxide nanoparticles (ZnO-NPs) and their incorporation into polymethyl methacrylate (PMMA) to produce PMMA/ZnO-NPs nanocomposites. The nanocomposites are prepared using the solution casting method, with ZnO-NPs mass contents varying between 1% and 7%. X-ray diffraction (XRD) analysis revealed a hexagonal wurtzite structure for ZnO–NPs, which formed a phase-separated structures with the PMMA matrix. Scanning electron microscopy (SEM) images showed that ZnO-NPS were homogeneously distributed throughout the PMMA polymer matrix and higher ZnO-NPs content led to increased particle size and agglomeration. Fourier transform infrared (FTIR) confirmed ZnO integration. UV-Vis spectra indicated that ZnO-NPs influenced the optical properties of PMMA, with ZnO-NPs/PMMA 3% composite showing the highest absorption and good nanoparticle dispersion. Thermogravimetric analysis (TGA) indicated enhanced thermal stability, with composites showing a 12 °C higher degradation temperature than pure PMMA. Photocatalytic performance was evaluated by degrading an azo dye (Acid Red) under UV light. Both ZnO–NPs and PMMA/ZnO-NPs composites achieved up to 99% dye removal at 10 mg/L within 2 h. According to the kinetic study, the photodegradation process followed pseudo-second-order model. Optimal dosages were 2.8 g/L for ZnO–NPs and 2 g/L for PMMA/ZnO-NPs composites. PMMA/ZnO-NPs composites demonstrated moderate recyclability over four cycles, making them suitable for sustainable water purification applications. This work highlights the potential of ZnO–NPs/PMMA as cost-effective, thermally stable, and efficient photocatalysts for environmental remediation.

Keywords Zinc oxide · Polymethyl methacrylate · Casting method · Water purification · Photocatalytic properties

✉ Bahri Deghfel
bahri.deghfel@univ-msila.dz

✉ Ahmad Azmin Mohamad
aam@usm.my

[1] Laboratory of Materials and Renewable Energy, Faculty of Sciences, University of Mohamed BOUDIAf -M'Sila, University Pole, Road Bourdj Bou Arreiridj, M'Sila 28000, Algeria

[2] Department of Chemistry, Faculty of Science, University Mohamed BOUDIAf -M'Sila, University Pole, Road Bourdj Bou Arreiridj, M'Sila 28000, Algeria

[3] Ecole Normale Supérieure de Boussaada, Boussaada 28201, Algeria

[4] Department of Physics, Faculty of Sciences, University of Mohamed BOUDIAf -M'Sila, University Pole, Road Bourdj Bou Arreiridj, M'Sila 28000, Algeria

[5] Laboratory Physico-Chemistry of Materials, Laghouat University, Laghouat 3000, Algeria

[6] Energy Materials Research Group (EMRG), School of Materials and Mineral Resources Engineering, Universiti Sains Malaysia, Pulau Pinang, Nibong Tebal 14300, Malaysia

Published online: 20 May 2025

Introduction

Environmental pollution, particularly in water sources, is significantly caused by organic dyes used in the food, cosmetics and textile industries [1, 2, 3]. Only10-20% of dyes with different degrees of toxicity are disposed of due to their resistance to degradation and treatment with organic and inorganic chemicals, leading to secondary pollution. This situation necessitates sustainable and chemical-free solution [1]. Nanotechnology offers practical solutions for water treatment as nanoscale materials (1–100 nm) display unique physical and chemical properties, enhancing surface reactivity and surface to volume ratio. An innovative purification method involves the combined use of nanostructures and photocatalysts [4].

Photocatalytic process have gained significant interest because they are sustainable, don't require chemicals and can mineralize dangerous pollutants in water. In contrast to other pollutant-transferring processes like adsorption, coagulation-flocculation, precipitation, ion-exchange, etc., photocatalysis is unique. Under UV or solar radiation, photocatalysts create reactive oxygen species (radicals or ROS), which can convert organic contaminants into CO_2 and H_2O in a process called mineralization [5, 6, 7]. In this process, inorganic semiconductors like zinc oxide (ZnO), titanium dioxide (TiO_2), iron(III) oxide (Fe_2O_3) vanadium(V) oxide (V_2O_5) and zirconia (ZrO_2) are used as photocatalysts [8, 9, 10]. ZnO, one of the many semiconductors under study, has gained attention as a promising option for photocatalytic uses because of its intrinsic qualities, including direct band-gap in the ultraviolet region, low cost, non-toxicity, environmental friendliness and great abundance [6]. ZnO exhibits an extensive absorption spectrum range, radiation hardness and chemical/thermal stability [11, 12]. Additionally, it has a good catalytic activity, an acceptable refractive index and strong antimicrobial properties [13]. ZnO has numerous applications including use in transparent electrodes for dye-sensitized solar cells, sensors, fillings in a variety of materials, UV photodetectors and light-emitting diodes [7], blue UV ray emitters and detectors, transparent high-power electronics [14], photoelectronic apparatuses [15] and water treatment including photocatalysis [12, 16].

The integration of ZnO at low percentages within polymer matrices enhances flexibility, formability, and cost-effectiveness, though the consolidation process is not yet fully understood [11]. Researchers are increasingly interested in hybrid materials that merge polymer-based and ZnO-based components for these benefits [4, 17, 18]. Several papers report on nano-ZnO coupled with various polymers, including poly(N-isopropylacrylamide), polyester, hybrid polymers, polyethylene glycol or Pluronic F127 [4], hyperbranched polyimide (HBPI) [19], poly(amide–imide) [20], polystyrene [21], high-density polyethylene composite [22], biocompatible poly(N -isopropylacryl- amide) (PNIPAAm) [23] and Cs/PVP blend [24]. Among the available polymers, poly(methyl methacrylate) (PMMA) is widely used in a variety of applications [4] due to its low cost, chemical stability, visible light transparency, hydrophobic qualities and favorable mechanical characteristics [6, 11, 25]. PMMA also exhibits a refractive index of $n = 1.49$; high mechanical flexibility, thermal stability, and chemical resistance [26, 27], as well as non-toxicity, excellent surface resistivity, low UV absorption and high thermal stability [28].

The novelty of this study, among other works, lies in the incorporation of low concentrations (1–7%) of ZnO nanoparticles into poly(methyl methacrylate) (PMMA) using the casting method. This approach enhances photocatalytic efficiency while maintaining cost-effectiveness. Unlike previous studies, our work emphasizes the improved thermal stability of PMMA through optimized ZnO-NPs dispersion. Furthermore, recyclability tests over four cycles demonstrate the long-term applicability of the PMMA/ZnO-NPs nanocomposites in water treatment. The inclusion of detailed kinetic modeling (pseudo-second-order), dosage optimization and exploring the optimal ZnO-NPs loading for enhanced photocatalytic performance further distinguishes this work, providing practical insights often overlooked in similar studies.

Materials and methods

Materials

Poly(methyl methacrylate) (PMMA) was purchased from Fisher Scientific [29]. Zinc acetate dihydrate [$Zn(CH_3COO)_2.2H_2O$], Chloroforme, sodium hydroxide (NaOH 2 M), and silver nitrate ($AgNO_3$) were also acquired from Fisher Scientific. The AR dye is an azo dye (Nylosan Red N-2RBL), with a molecular weight of 587.97 g mol^{-1} and a solubility of 80 g L^{-1} [30], was acquired from Varian. UV lamp (Model VL-6.C,6 W-254 nm tube, 230 V 50/60Hz, power:12 W, made in France) was used for the photocatalytic degradation of AR dye and the generation of hydroxyl radicals.

Synthesis of ZnO-NPs

A 0.46 M solution of zinc acetate dihydrate [$Zn(CH_3COO)_2.2H_2O$] was prepared by dissolving it in 150 mL of distilled water at 50–55 °C. The solution was then stirred for two hours, and the pH was gradually increased from 5.7 to 9.0 by adding 70 mL of 2 M NaOH. The reacted mixture was stirred until a chemically homogeneous

solution was achieved, resulting in a milky white precipitate, which was then separated by centrifugation at 4000 rpm for 20 min. It was dried for 15 h at 110 °C in an oven, then calcined by heating rate of 15 °C/min for 2.5 h at 450 °C. The product was repeatedly rinsed using distilled water until clear, verified with $AgNO_3$ testing (absence of precipitation), and centrifuged at 4000 rpm for 20 min each time. Next, it was dried for 24 h at 80 °C, ground in a mortar, and sieved to a particle size of less than 90 µm. The resulting ZnO nanopowder was recovered and identified by SEM, XRD, FTIR, and TGA.

Preparation of PMMA/ZnO-NPs nanocomposites

To prepare the nanocomposite samples, initial solutions were formed by dissolving PMMA granulate (3.96, 3.88, 3.80 and 3.72 g) in 25 mL of chloroform solvent and stirring for one hour at 25 °C. Separately, ZnO solutions (0.04, 0.12, 0.2 and 0.28 g) were prepared in 25 mL of chloroform solvent under the same stirring conditions. Then, the PMMA solutions were added to the ZnO solutions and mixed for three hours at 40 °C to evaporate the solvent, yielding ZnO/PMMA nanomaterials with ZnO contents of 1%, 3%, 5% and 7%. The prepared samples were ground using an agate mortar and sieved to obtain a particle size of less than 90 µm before further characterization. The resulting nanocomposites were identified by SEM, XRD, FTIR, and TGA.

Photocatalytic degradation

AR dye (Nilosan Red N-2RBL) was selected for photodegradation. First, the catalysts (ZnO-NPs or ZnO-NPs/PMMA)/ dye suspensions were stirred slowly in the dark for 30 min to ensure that the catalysts powders and acid red dye were well mixed and had reached equilibrium. Then, the suspnsions were placed in a dark box under the UV light positioned at a height of 10 cm (UV lamp with a wavelength of 254 nm, power of 12 W) and stirred using multiple magnetic stirrers at a speed of 300 rpm. The characteristic absorbance of AR at 501 nm was used to calculate the decomposition ratio.

The synthesis processes of ZnO-NPs and PMMA/ZnO-NPs nanocomposites are comprehensively summarized in Fig. 1. This figure outlines the preparation methods, materials involved, and their integration, offering a clear depiction of how these nanomaterials are fabricated for enhanced dye degradation efficiency.

Characterizations

The properties of the obtained samples were determined using different conventional techniques. XRD analysis was conducted with an X'Pert PRO MPD diffractometer. FTIR measurements were performed using a SHIMADZU IRSpirit QATR-S spectrometer. Absorbance measurement was examined using UV-vis −2401 PC-Shimadzu, Japan. SEM images and data were obtained using a Quattro ESEM system. TGA was performed using SDT Q600 TATGA, under a nitrogen flow rate of 10 mL/min, with a heating rate of 10 °C/min and a temperature range of 25 to 600 °C.

Results and discussion

Morphology study

Figure 2 shows SEM pictures of pure ZnO-NPs and PMMA/ZnO-NPs nanocomposites with varying ZnO content (1–7%). The SEM image confirms the successful incorporation of ZnO nanoparticles within the PMMA matrix, with an estimated average particle size of approximately 97 nm (Imagej software [31]). The nanoparticles appear well-dispersed, with some agglomeration, indicating that the nanocomposite maintains its nanoscale features. The surface of PMMA polymer appears smooth and highly viscous [2, 32, 33]. The surface of the ZnO layer looks to be made up of tiny granules [11], which accumulate in abundance because of the high surface energy of the nanoparticles [34]. The latter exhibit a narrow size distribution and can form various morphologies, including cubic or hexagonal shapes [35], rod-like formations [29], spindle-shapes with existence spherically deformed particles [7, 8]. Incorporating ZnO-NPs into the PMMA polymer matrix alters the morphological surface of the as-prepared products. The ZnO nanoparticles are homogeneously distributed throughout the polymeric matrix. With increased ZnO content, particle size tends to increase [2, 32], which increases its good dispersion [34]. Furthermore, the agglomeration of ZnO nanoparticles within the polymer matrix results from enhanced particles interaction due to the increased ZnO loading [35]. The addition of ZnO-NPs also increases the hydrophilicity of the particles, making them more porous and giving the impression of having a somewhat smooth surface [33].

Two main factors contribute to the agglomeration of ZnO particles: (1) the high concentration of particles in a limited volume of the polymer matrix; and (2) the formation of Zn–O–Zn linkages between particles. This is evident in the microscopic images shown in Figs. 2 for PMMA/ZnO-NPs nanocomposites with varying ZnO content of 1, 3 and 5% [35]. As the ZnO-NPs content increases from 1 to 5%, the nanocomposite surface becomes rougher, with some tiny particles accumulated as white spots of ZnO on the surface. This accumulation demonstrates adhesion between

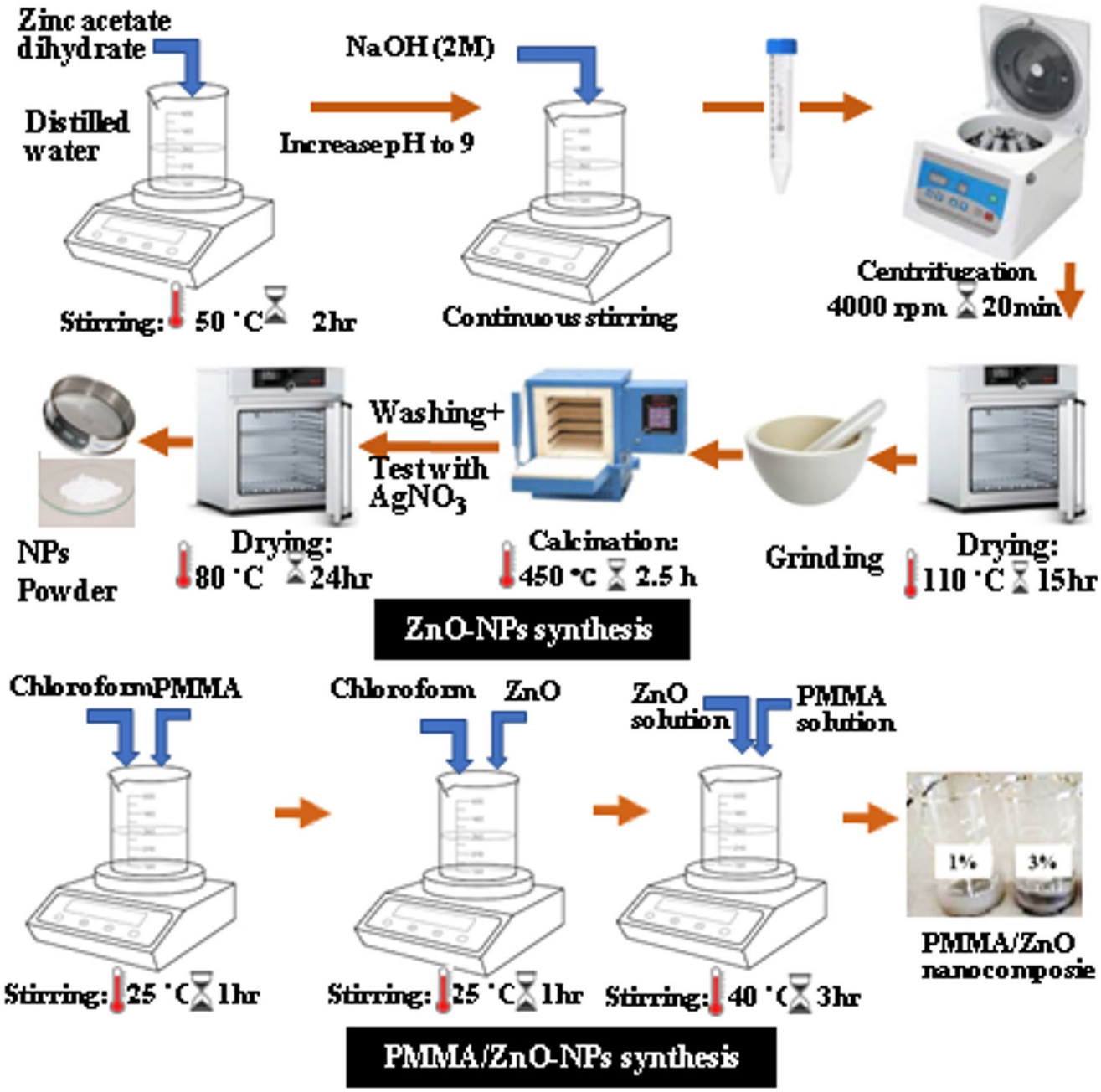

Fig. 1 Synthesis procedure of ZnO-NPs and ZnO-NPs/PMMA nanocomposites

ZnO-NPs and the PMMA polymer matrix, alongside some degree of separation in the polymeric system [3, 32].

Phase analysis

Figure 3**(a)** displays the XRD spectra of pure ZnO-NPs, PMMA and PMMA/ZnO-NPs nanocomposites with varying ZnO amounts (1–7%). The amorphous nature of PMMA is evident in the XRD pattern, where a broad peak appears at $2\theta = 13.38°$, due to the presence of a bulky pendant ester group in the chain [9, 36, 37]. As the ZnO content in the PMMA matrix rises, the intensity of peaks associated with ZnO becomes more noticeable [37, 38, 39]. In contrast, the broad amorphous peak of the nanocomposite becomes weaker due to its interaction with ZnO. This interaction reduces intermolecular contact and decreases the degree of crystallinity of the amorphous region [24].

The XRD pattern indicates that the ZnO nanoparticles resemble the hexagonal Wurtzite structure, with most diffraction peaks matching the JCPDS 36-1451 data [39, 40,

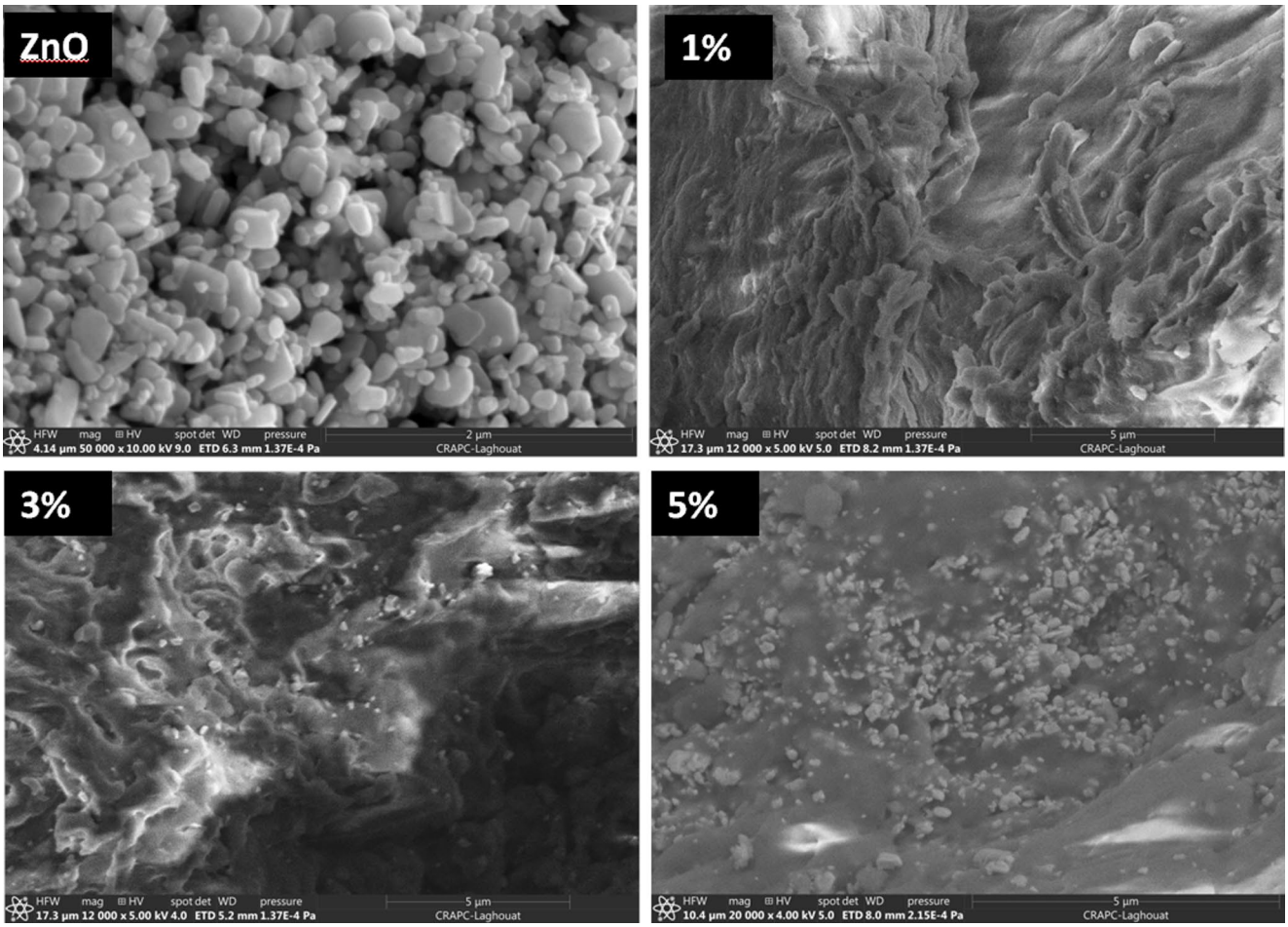

Fig. 2 SEM results of ZnO and PMMA/ZnO-NPs nanocomposites with varying ZnO content of 1%, 3% and 5%

41]. As shown in Fig. 3**(a)**, a series of plane-derived diffraction peaks for ZnO are observed at (100), (002), (101), (102), (110), (103), (200), (112), (201), (004), and (205) corresponding to 2θ values of 28.66°, 31.03°, 31.80°, 32.68°, 34.45°, 36.28°, 42.74°, 47.57°, 50.75°, 56.62°, 60.69°, 62.89°, 66.40°, 67.98°, 69.11°, 72.60° and 76.98° [24, 38, 39, 42]. ZnO nanoparticles incorporated into the PMMA matrix does not alter or create new diffraction peaks, nor does it eliminate any PMMA peaks. Figure 3**(b)** displays the main characteristic peaks of ZnO wurtzite structure for PMMA/ZnO-NPs nanocomposites with varying ZnO amounts (1–7%). The intensity of these peaks increases with increasing the ZnO amount. Because of the strong boundaries between the C=O groups in the PMMA matrix and Zn^{2+} ions, the ZnO-NPs-filled PMMA composite displays phase-separated structures [36, 37, 38].

Bonding analysis

Figure 4 shows the FTIR spectra for pure PMMA, ZnO-NPs, and PMMA/ZnO-NPs nanocomposites. Table 1 lists the characteristic bonds identified for these compounds [38, 29]. The characteristic peaks of pure PMMA appear at wavenumbers 474, 752, 987, 1141, 1190, 1238, 1387, 1436, 1722, 2951, and 2995 cm^{-1} [29]. The distinct peak located between 1120 and 1010 cm^{-1} is attributed to the stretching vibration of C=O=C in PMMA [13]. The band at 1722 cm^{-1} represents the distinctive peak of PMMA, which is associated with the carbonyl (C=O) group [33, 43, 44].

After preparing the PMMA/ZnO-NPs nanocomposites, a shift in the stretching vibration of C=O group from 1722 cm^{-1} to 1725 cm^{-1} was observed due to the incorporation of ZnO into the PMMA matrix. The presence of ZnO-NPs is confirmed by distinctive peaks at 474,460 and 444 cm^{-1} [13, 29, 45], which correspond to the stretching vibration of the Zn-O bonds and become more pronounced with increased ZnO doping [43].

Additionally, sp^2 C-H bonds are observed at 2951 and 2995 cm^{-1} [29, 43], whose intensity increases due to the interaction between ZnO-NPs and PMMA matrix [43]. The FTIR spectra of both PMMA and PMMA/ZnO-NPs nanocomposites confirm the presence of all characteristic bonds,

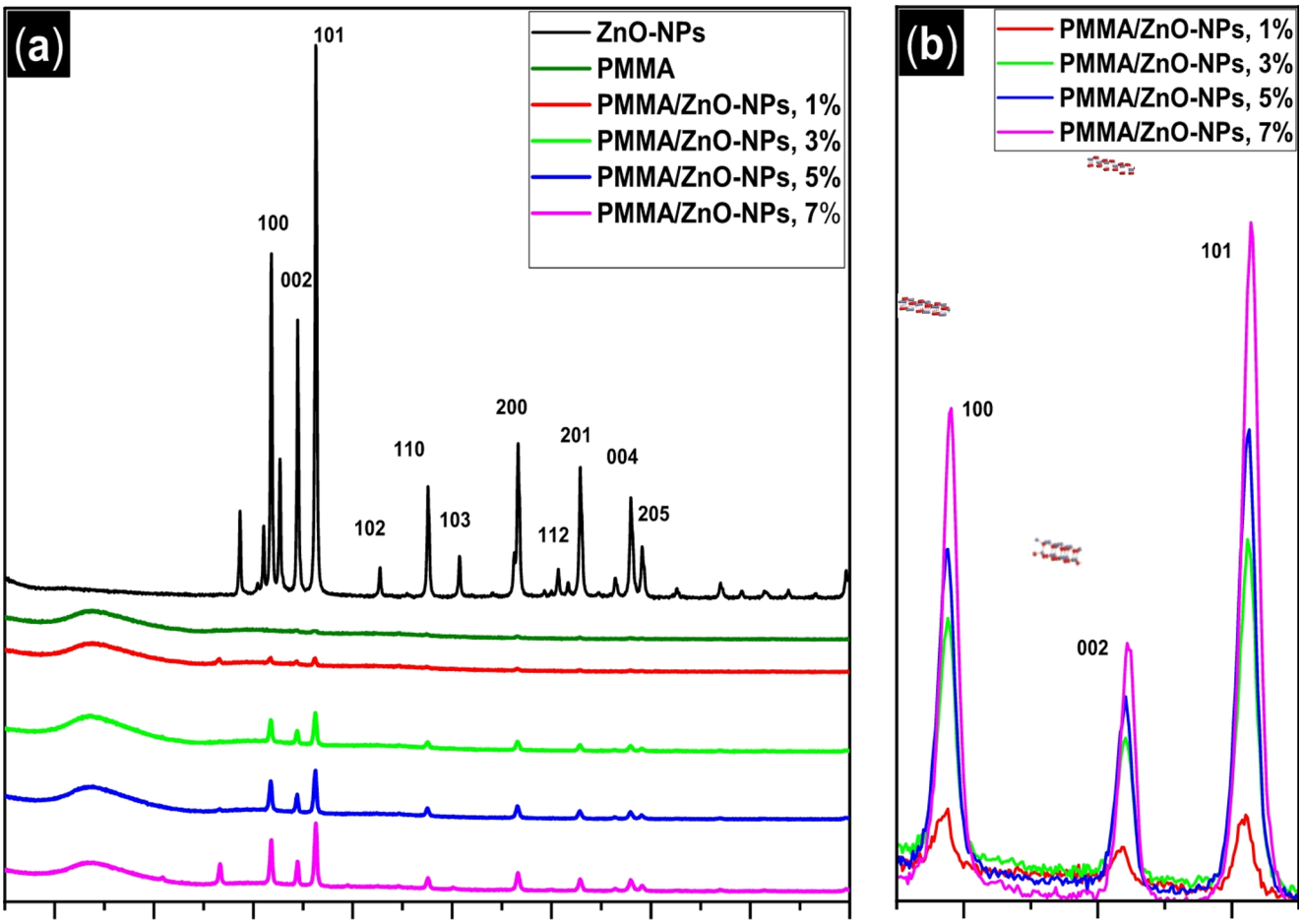

Fig. 3 **(a)** XRD patterns of pure ZnO, PMMA and PMMA/ZnO-NPs nanocomposites samples, **(b)** main characteristic peaks of ZnO wurtzite structure for PMMA/ZnO-NPsnanocomposites with varying ZnO amounts (1–7%)

indicating that the addition of ZnO does not affect the chemical structure of the polymer [38]. The wide peak located between 3200 and 3700 cm^{-1}, specifically at 3675 cm^{-1}, is ascribed to the stretching vibration caused by the OH groups on the ZnO-NPs surface, likely due to residual water and sodium hydroxide used during synthesis [13, 35]. The disappearance of the OH vibration peak at 3% ZnO is likely due to optimal nanoparticle dispersion and strong ZnO-PMMA interactions, leading to complete hydroxyl passivation. At other concentrations, either insufficient embedding (1%) or nanoparticle agglomeration (5%, 7%) allows hydroxyl groups to remain detectable [46].

Thermal analysis

Thermogravimetric analysis (TGA) of pure PMMA and PMMA/ZnO-NPs nanocomposites is shown in Fig. 5a. The thermal degradation of the nanocomposites occurs in three steps [45], involving the scission of H–H linkage at 181 °C with mass loss of 1.35%, the vinylidene end group, and random scission of the polymer main chain at 389 °C with mass loss of 97.42% [37].

The thermal stability of PMMA improved by incorporating ZnO-NPs at filler contents of 1, 3, 5 and 7 wt% ZnO. Three decomposition steps are observed with ZnO incorporation. The first decomposition step occurs within the range of 100–230 °C [14, 45], with mass loss of 3.78%, 5.14%, 3.36% and 5%, represented by DTG peak at 143 °C, 176 °C, 154 °C and 183 °C, respectively (Table 2). This is attributed to the evaporation of residual solvent and probably the depolymerization step initiated at weak head-to-head linkages, formed by combination of vinylidene chain ends from disproportionation [14, 47].

The second decomposition step occurs within the range of 230–300 °C [14, 45], with mass loss of 2.66%, 3.67%, 2.48% and 5.45%, corresponding to the decomposition of terminal vinyl groups [14]. The third main decomposition step occurs within the range of 300–450 °C [14, 45], with mass loss of 90.81%, 87.79%, 85.94% and 76.82%, represented by the DTG peak at 393 °C,393 °C, 394 °C and 401 °C, respectively (Table 2). According to the derivative

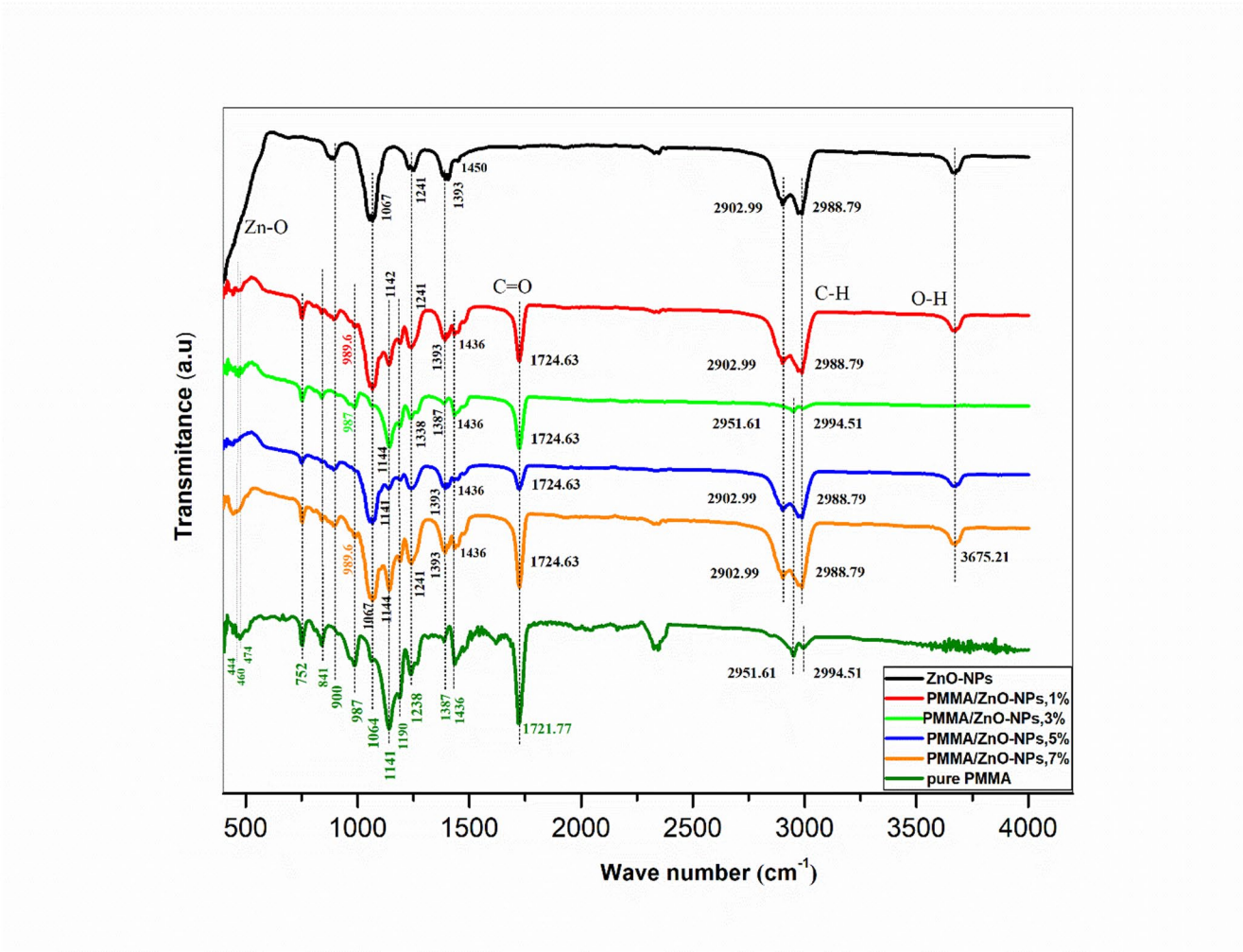

Fig. 4 FTIR spectra of pure PMMA, ZnO-NPs and PMMA/ZnO-NPs nanocomposites samples

Table 1 Main bands appeared in PMMA/ZnO-NPs samples from FTIR spectra with their corresponding attributions

Wave numbers (cm^{-1})	Assignments
2995	Stretching mode in PMMA CH_2
2951	Stretching mode in PMMA C–H
1722	Stretching vibration of C = O group of ester
1436	Asymmetric bending mode in PMMA O–CH3
1387	Twisting mode in PMMA CH_2
1238	C-O stretching vibration
1190	Stretching mode O–CH_3 in PMMA
1141	C-O-C vibration of the methoxy group of PMMA
987	C-C stretching of PMMA
841	C-O-C stretching vibration
752	Bond CH_2
444, 460	Characteristic peaks of ZnO
474	Zn–O in ZnO

thermogravimetry (DTG) peak (Fig. 5b), the decomposition initiated by random scission of the polymer backbone due to the transfer of radicals to unsaturated chain ends [14, 47].

The main random chain scission increases from 389 °C in neat PMMA to 401 °C in 7 wt% ZnO, due to the ability of nanoparticles to prevent volatile degradation products. Two mechanisms explain this increase: first, steric obstructs the motion of polymer chains, which lowers the chain scission-promoting interactions with surrounding moieties and thermally induced strain on the polymer backbone [37]. The second mechanism involves the localization of charge from ZnO-NPs surfaces (the charge arising from the carbonyl dipole), which may promote bond scission and destabilize polymer units, including vinylidene decomposition. Both mechanisms thus involve disruption of the chemical and physical environment of the polymer [37, 45].

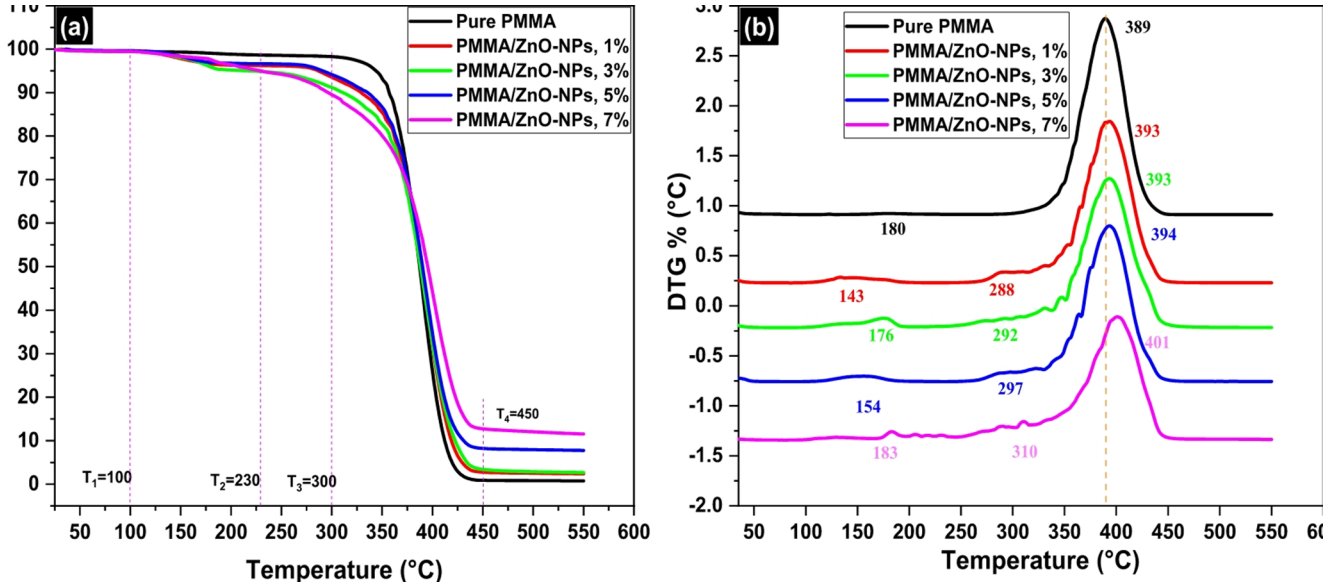

Fig. 5 **(a)** TGA curves and **(b)** their corresponding DTG curves of pure PMMA and PMMA/ZnO-NPs nanocomposites

Table 2 TG/DTG results of PMMA/ZnO-NPs nanocomposites

Sample	Step1	100–230 °C	Step2 230–300 °C	Step3	300–450 °C	Residue
	Wt% loss	DTG	Wt % loss	Wt % loss	DTG	Wt%
Pure PMMA	1.35	180	0.36	97.42	389	0.87
PMMA/ZnO(1%)	3.78	143	2.66	90.81	393	2.75
PMMA/ZnO(3%)	5.14	176	3.67	87.79	393	3.4
PMMA/ZnO(5%)	3.36	154	2.48	85.94	394	8.22
PMMA/ZnO(7%)	5	183	5.45	76.82	401	12.73

Optical properties

UV-Vis spectroscopy (190–1100 nm) reveals that embedding ZnO nanoparticles into a PMMA matrix significantly alters the composite's optical properties (Fig. 6). ZnO, with a direct bandgap of ~3.37 eV, strongly absorbs in the UV region, making it suitable for photocatalysis [48]. In addition to the intrinsic absorption edge near 368 nm (3.37 eV), a broader absorption feature around 450–500 nm was observed, which can be attributed to sub-bandgap transitions involving intrinsic defects (e.g., oxygen vacancies or zinc interstitials) commonly present in ZnO nanostructures [48]. PMMA, being highly transparent, reduces the overall absorbance when used as a matrix. Among the composites, ZnO-NPs/PMMA 3% exhibits optimal light absorption, suggesting well-dispersed nanoparticles with minimal aggregation. This uniform dispersion enhances UV absorption and promotes efficient charge separation, thereby improving photocatalytic activity. In contrast, higher loadings (5% and 7%) tend to induce nanoparticle agglomeration, decreasing the active surface area and reducing photocatalytic efficiency [49].

Photodegradation of acid red dye by UV irradiation

The photodegradation performance of ZnO-NPs and PMMA/ZnO-NPs nanocomposites was evaluated by degrading AR dye in water under UV irradiation. The percentage degradation of AR dye was determined using the following relationship:

% of Degradation = $(C_0 - C_t)/C_0 \times (100\%) = (A_0 - A_t)/A_0 \times (100\%)$,

where C_0 and C_t are the initial dye concentration and concentration after irradiation, respectively, and A_0 and A_t are the corresponding initial absorbance and absorbance after irradiation [50, 51, 52]. Parameters affecting the degradation such as catalyst dosage, initial dye concentration, contact time and recycling process, were investigated.

Effect of catalyst dosage (loading(on the degradation rate of AR dye

The effect of catalyst dosage on the degradation rate of AR dye was investigated by varying the catalyst amount from 0.4 g/L to 4 g/L under the following conditions: pH = 7, temperature = 22 °C, contact time t = 2 h, C_0 = 20 mg/L, and volume = 25 mL. The UV–Vis absorbance spectrum of AR dye,

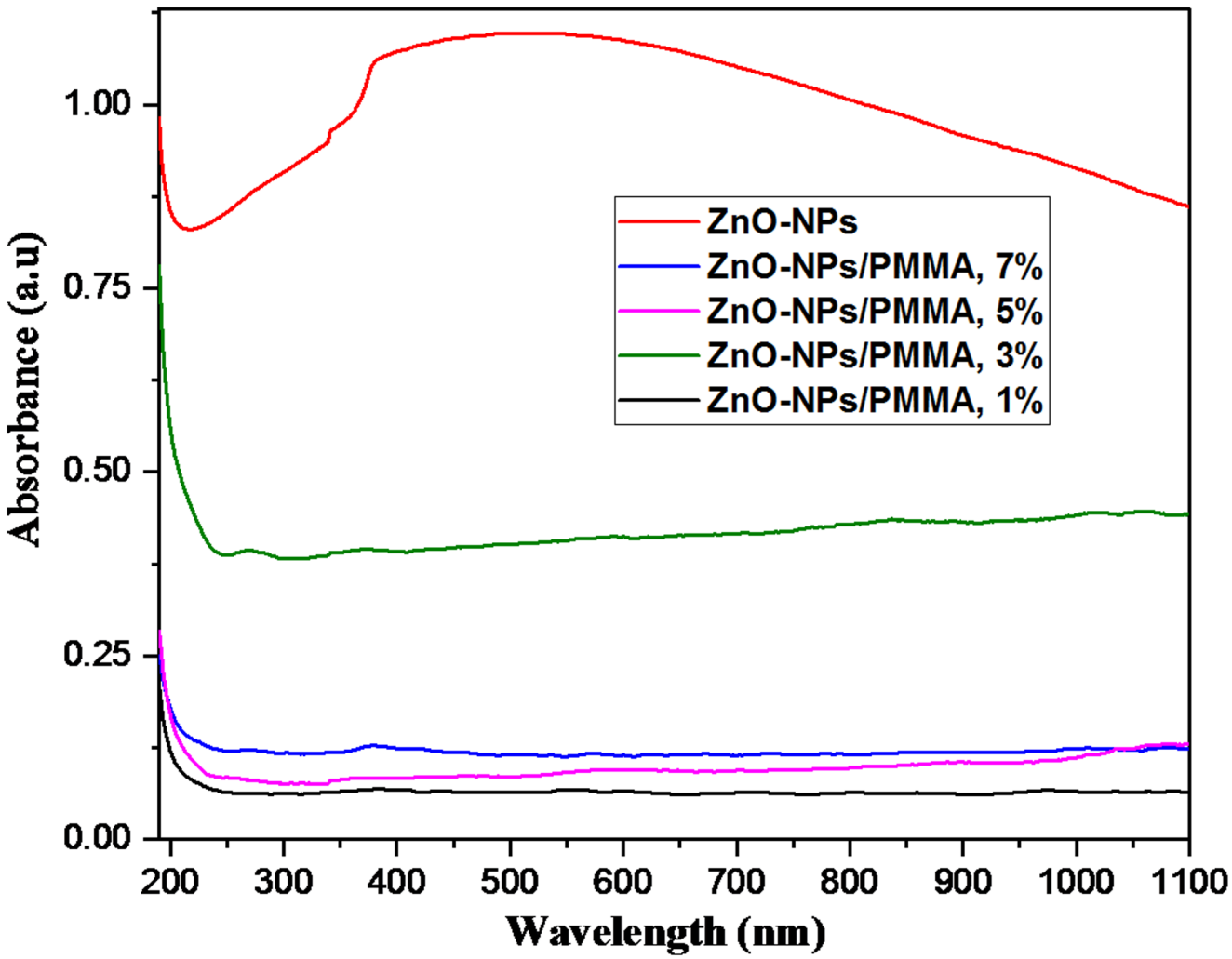

Fig. 6 Absorbance spectra of PMMA/ZnO-NPs nanocomposites

shown in the inset of Fig. 7, exhibits a broad peak around 500 nm. Figure 7 shows that the degradation rate of AR dye increases significantly with increasing catalyst dosage, after which it begins to stabilize and then slowly decreases. The highest AR dye degradation rate for pure ZnO-NPs was 80.55% at a dosage of 2.8 g/L. For 1% and 7% ZnO contents in PMMA matrix, the degradation rate initially increases to 52.45% and 50.5%, respectively, at 2 g/L dosage, then it begins to stabilize and slowly decreases to 51.3% and 47% at 4 mg/L dosage. This suggests that the optimum dosage of ZnO-NPs is 2.8 g/L, and for PMMA/ZnO-NPs1% and 7% contents, it is 2 g/L. The initial amount of the solute influences the optimum catalyst loading, since an increase in dosage results in more active surfaces and more active sites on the catalyst surface. However, at higher photocatalyst dosages, light dispersion occurs, which reduces UV light penetration and photoactivated suspension volume, rendering them inappropriate under low irradiance or group lighting [53, 54, 55]. This drop in the rate of AR dye mineralization above the 2.8 g/L and 2 g/L dosage limiting values is attributed to the increased turbidity of the solution after UV light exposure, which inhibits photon energy absorption necessary for generating more hydroxyl radicals [56].

Effect of AR dye concentration

The effect of AR dye concentration on the degradation efficiency was investigated by varying the AR dye concentration from 10 mg/L to 40 mg/L under the following conditions: pH = 7, temperature = 22 °C, t = 2 h, catalyst mass m = 50 mg, and volume = 25 mL. Our results (Fig. 8**(a)**, **(b)**, **(c)**) indicate a continuous decrease in the degradation rate with increasing initial concentration of AR dye from 10 to 40 mg/L, as follows: from 99.9 to 67.45% for ZnO-NPs and to 63.55% and 60.62% for PMMA/ZnO-NPs1% and 7%, respectively. The photocatlytic observations of dye solution with various initial concentrations are shown before treatment (Fig. 8(**d**), (**e**), (**f**)) and after treatment (Fig. 8(**g**), (**h**),

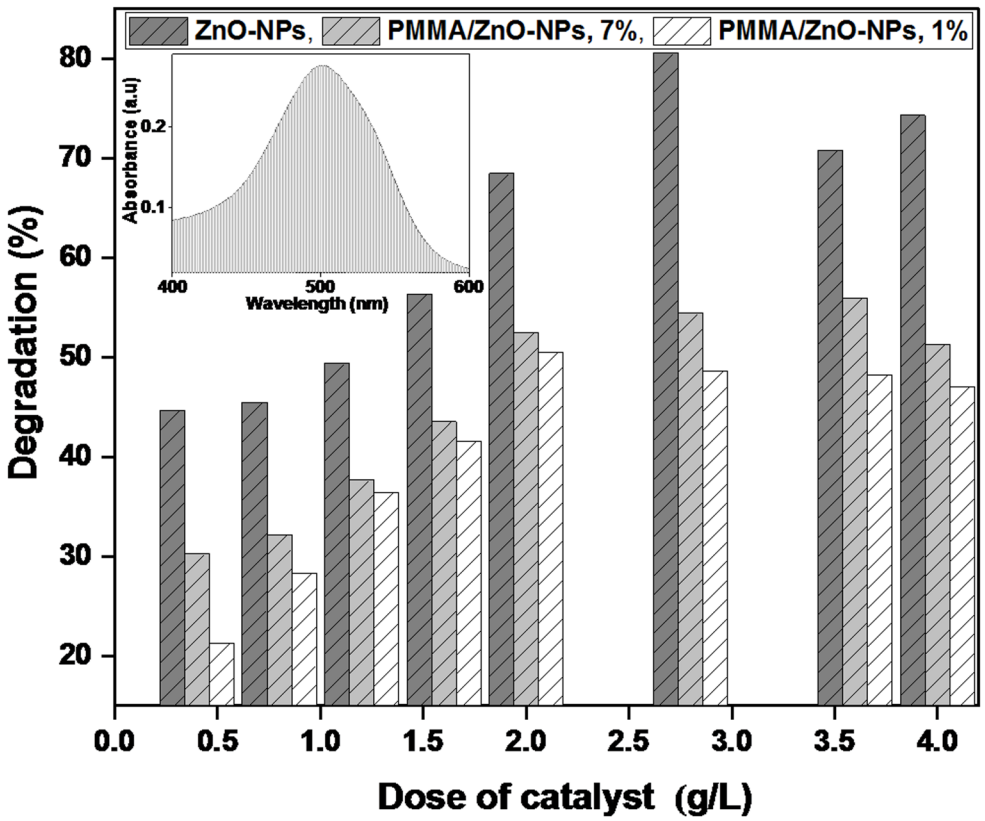

Fig. 7 Effect of catalyst dosage on percentage degradation of AR dye. Inset shows UV-vis absorbance of AR dye

(**i**)) for ZnO-NPs, PMMA/ ZnO-NPs 7%, and PMMA/ ZnO-NPs 1% nanocomposites samples. The observed decrease in the degradation rate is attributed to the intensified color of the dye mixture at higher initial concentrations, leading to increased opacity and light scattering. Consequently, photon penetration into the dye is decreased, preventing light from reaching the catalyst surface and reducing the number of active sites, thereby decreasing the degradation rate [55, 57].

The degradation efficiency is inversely proportional to the dye concentration, with lower concentrations increasing the degradation efficiency due to the greater surface area on the photocatalyst. However, higher concentrations reduce the generation of OH• free radicals due to the dye molecules adsorbed on the catalyst surface, which decreases the degradation efficiency [54, 58, 59].

The PMMA/ZnO-NPs nanocomposites achieved 99.9% AR dye degradation in 120 min (Table 3), outperforming other ZnO-polymer systems [4, 6, 11, 40, 43, 60, 61, 62, 63]. ZnO/PANi@PMMA degraded 91% of methyl orange in 140 min [40], while ZnO-MoS_2-PMMA films reached 75% RhB degradation in 240 min [6]. The enhanced performance of PMMA/ZnO-NPs is likely due to optimal ZnO dispersion and strong ZnO-PMMA interactions, making it a promising photocatalyst for wastewater treatment.

Effect of contact time

The effect of contact time on AR dye degradation is investigated under the following conditions: pH = 7, temperature = 22 °C, catalyst mass m = 50 mg, volume = 25 mL, and initial AR dye concentration = 20 mg/L. The contact time is varied from 0 to 120 min in photocatalytic and photolytic tests (Fig. 9**)**. Before irradiation (t < 0 min: under dark conditions), a small initial amount in dye elimination efficiency is observed, which can be attributed to the adsorption of AR dye onto the surface of ZnO-NPs and PMMA/ZnO-NPs nanocomposites. At 45 min, the AR dye removal percentage reaches 70.4% for ZnO and 35.3%, 37.65%, 36.85 and 34.6% for 1%, 3%, 5% and 7% contents, respectively, as shown in Fig. 9a. In the range from 0 to 45 min, the degradation rate is rapid due to the increased generation of free radicals from electron excitation by the catalysts, indicating that more active binding sites are available on the catalyst surface [60, 64]. The optimum irradiation time was determined to be 45 min, which also happens to be the maximum adsorption rate occurred before reaching equilibrium. After 45 min, no significant increase in the degradation is observed, and the number of equilibrium sites is minimized. This implies that binding controls the adsorption [64]. The PMMA/ZnO-NPs nanocomposites exhibit moderate photocatalytic activity, with performance slightly affected by ZnO nanoparticle content. Notably, the ZnO-NPs/PMMA

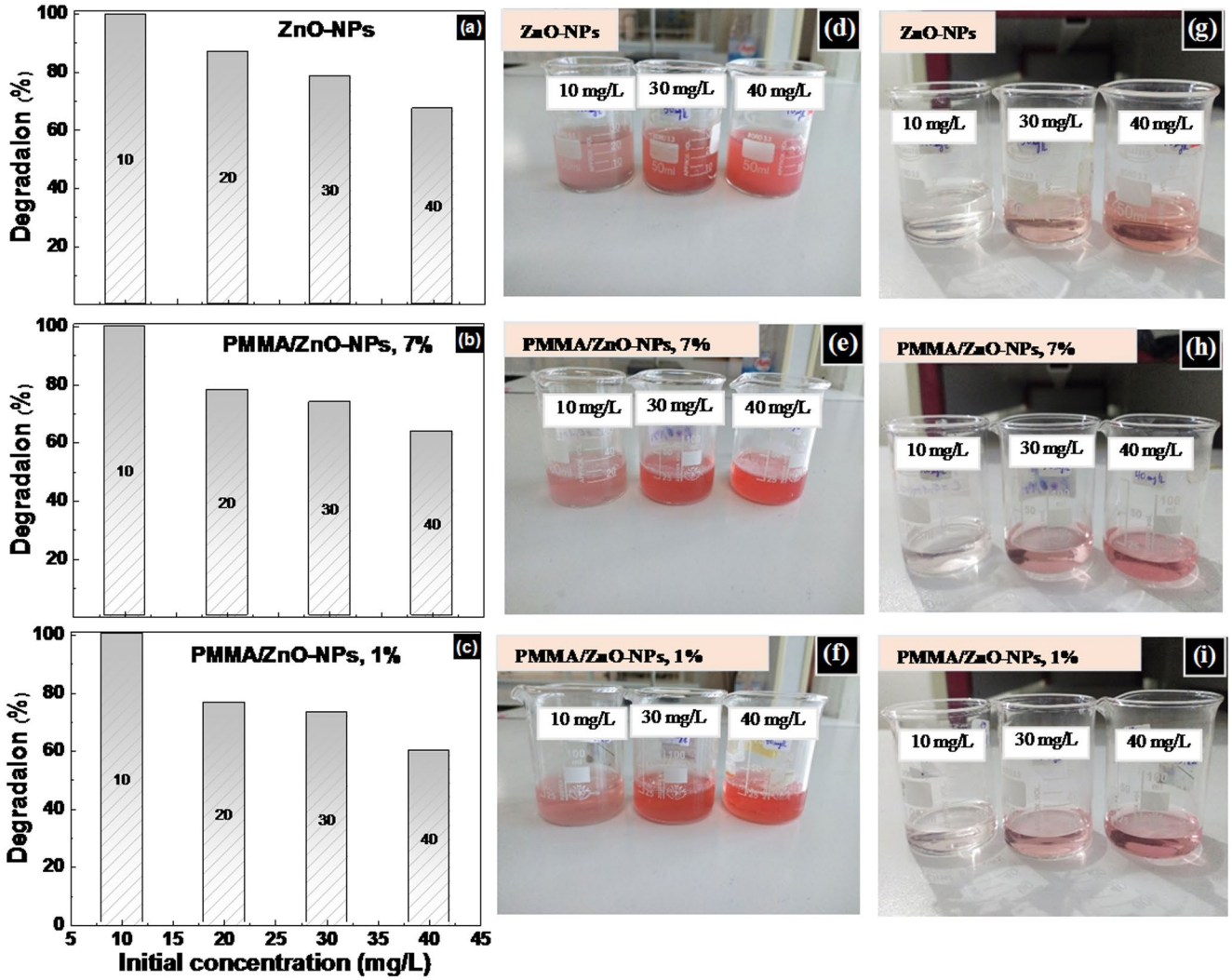

Fig. 8 Effect of initial AR dye concentration on the degradation efficiency for (**a**) ZnO-NPs, (**b**) PMMA/ ZnO-NPs 7%, and (**c**) PMMA/ ZnO-NPs 1% nanocomposites samples. Photocatlytic observations of dye solution with various initial concentration before treatment are shown in (**d**), (**e**), (**f**) and after treatment in (**g**), (**h**), (**i**), respectively

Table 3 Comparison of photocatalytic degradation efficiencies of various ZnO-based polymer nanocomposites for organic dye removal

Nanocomposites	Dye	Content	Volume	Catalyst dosage	Time (min)	Degradation (%)	Radiation
Our results: ZnO-NPs PMMA/ZnO-NPs	AR	10 mg/L	25 ml	2 g/L	120	99.9%	UV lamp (254 nm)
Nitrogen doped ZnO [**60**]	NPX	2 mg/L	500 ml	0.35 g/l	180	89%	Sunlight
ZnO/PANi@PMMA [**40**]	MO	15 mg/L	100 ml	ZnO/PANi@PMMA coated leaf mesh	140	91%	Sunlight
ZnO/PMMA **[4]**	MB	1.5×10^{-5} M	2 ml	100 mg	240	~60%	UV lamp (368 nm)
ZnO/PMMA [**43**]	MB	10 µM	--	ZnO/PMMA thin film	100	96%	Sunlight
ZnO-MoS2-PMMA **[6]**	RhB	1.5×10^{-5} M	2 mL	1cm^2 film (ZnO-PMMA and ZnO-30% MoS2-PMMA)	240	~55–75%	LED UV lamp (365 nm)
ZnO/PMMA [**11**]	MB	1.5×10^{-5} M	4 mL	ZnO Solution Casting	240	~67%	UV lamp (365 nm)
PAN@ZnO [**61**]	MB	(10 mg/ml)	50 mL	50 mg	60	65%	Mercury lamp 50 W
ZnO/Polystyrene [**62**]	MB	45 mg/L	15 mL	0.1 g	150	42%	UV lamp (365 nm)
EPS/ZnO [**63**]	MB	20 ppm	5 mL	0.014 g	20 h	45%	UV light

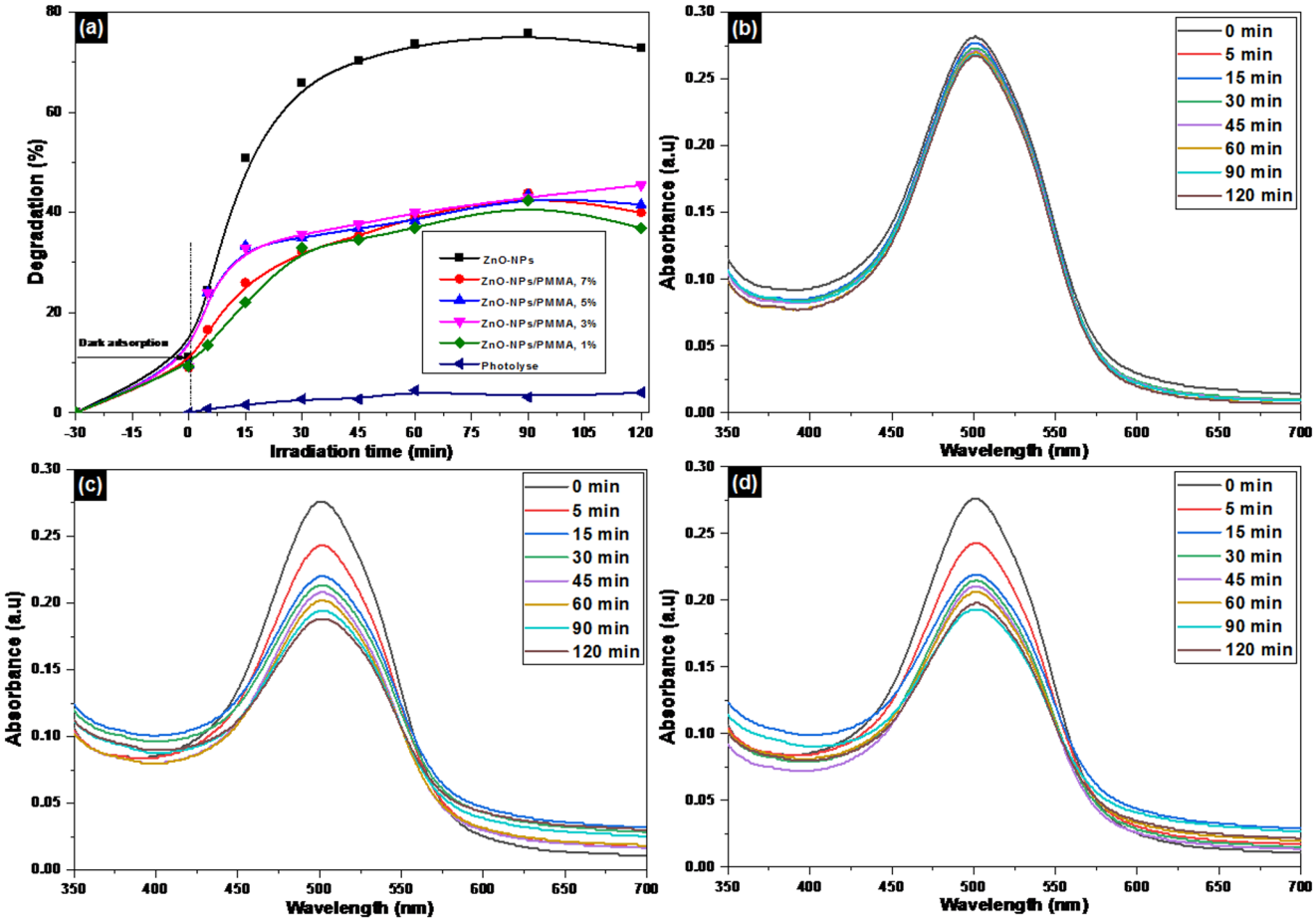

Fig. 9 **(a)** effect of contact time on the photocatalytic and photolytic degradation efficiency of AR dye, (**b**) UV-vis absorbance for photolytic degradation, and photocatalytic degradation using PMMA/ZnO-NPs nanocomposites with ZnO-NPs content of (**c**) 1% and (**d**) 7%

composite with 3% ZnO demonstrates the highest photocatalytic efficiency, aligning well with its superior light absorption observed in the UV-Vis spectra.

On the other hand, to assess the photocatalytic contribution of the ZnO-NPs and ZnO-NPs/PMMA nanocomposites, a control experiment was performed by exposing the AR dye solution to UV light (254 nm, 12 W) without the photocatalyst, indicated as photolyse in Fig. 9a. The photolytic degradation under these conditions is minimal, confirming that self-degradation due to light exposure is negligible. UV-vis absorbance spectra are also presented as representative data for photolytic degradation (Fig. 9b) and photocatalytic degradation using PMMA/ZnO-NPs nanocomposites with ZnO-NPs contents of 1% (Fig. 9c) and 7% (Fig. 9d). These spectra clearly illustrate the degradation process, with a slight reduction in the characteristic absorption peak of AR dye under UV irradiation for photolytic degradation, whereas photocatalytic degradation exhibits a pronounced decrease, confirming the enhanced dye removal efficiency of the ZnO-PMMA nanocomposites.

Kinetic models of photocatalysis

Kinetic analysis is important since it shows the rate at which AR degrades and, consequently, the amount of time needed for the reaction to finish. The pseudo-zero-order kinetics model is used when the reaction rate is independent of the reactant concentration, often due to catalyst surface saturation or limited light absorption. The rate equation is: $C_t = C_o - k_0.t$, where C_t is the pollutant concentration at time, C_o is the initial concentration, and k_0 is the rate constant. A linear plot of C_t vs. t confirms pseudo-zero-order behavior, with the slope equal to $-k_0$(Fig. 10a**)** [51]. The pseudo-first-order kinetic model postulates that the rate of concentration change of AR dye is exactly proportional to its remaining concentration over time, as the number of degrading molecules is minimal compared to the catalyst population [51]. The rate equation used is: $ln(C_o/C_t) = k_1.t$, where C_0 is the initial concentration, C_t is the concentration at time t, k_1 is the apparent first-order rate constant. k_1 is determined from the slope of the plot of $-\ln C_t/C_0$ vs. t **(**Fig. 10b**)**, indicating the rate of photocatalytic degradation (min^{-1}), with a higher

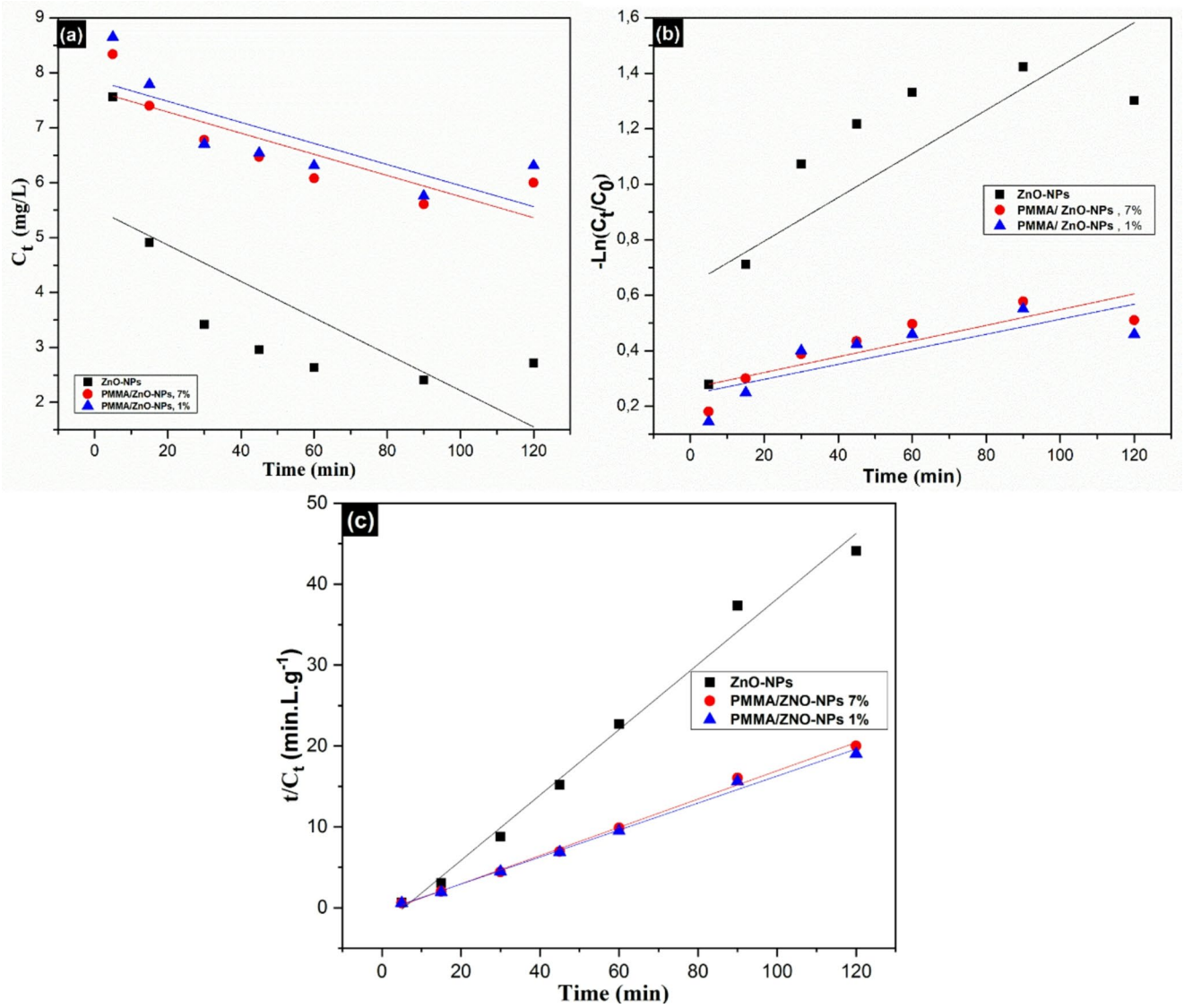

Fig. 10 **(a)** pseudo-zero-order, **(b)** pseudo-first-order, **(c)** pseudo-second-order degradation kinetic model

Table 4 Kinetic modeling results for the degradation of AR dye using ZnO-NPs and PMMA/ZnO-NPs nanocomposites

Sample	pseudo-zero-order		pseudo-first-order		pseudo-second-order	
	k_0 (mg/L.min)	R^2	k_1 (min^{-1})	R^2	k_2 (L/g.min)	R^2
ZnO-NPs	0.033	0.737	0.007	0.789	0.404	0.994
PMMA/ZnO-NPs 1%	0.019	0.846	0.002	0.859	0.166	0.998
PMMA/ZnO-NPs 7%	0.019	0.791	0.002	0.801	0.174	0.997

k_1 implying a faster reaction [7, 65]. The pseudo-second-order model is represented by the equation: $(1/C_0) - (1/C_t) = k_2 t$, where C_0, C_t and k_2 are the initial concentration, equilibrium concentration and second-order apparent rate constant, respectively. A plot of (t/Ct) vs. t gives a straight line (Fig. 10c), and the gradient of the slope is used to determine k_2 [51].

The modeling results in Table 4 indicate that the adsorption kinetics are best described by the pseudo-second-order model, showing a high correlation coefficient ($R^2 \approx 0.99$). In contrast, the pseudo-zero and first-order models yield lower correlation coefficients, making them less suitable for all samples.

Cyclic stability

Cyclic stability is one of the most important properties of a photocatalyst. The cyclic stability of ZnO-NPs and PMMA/

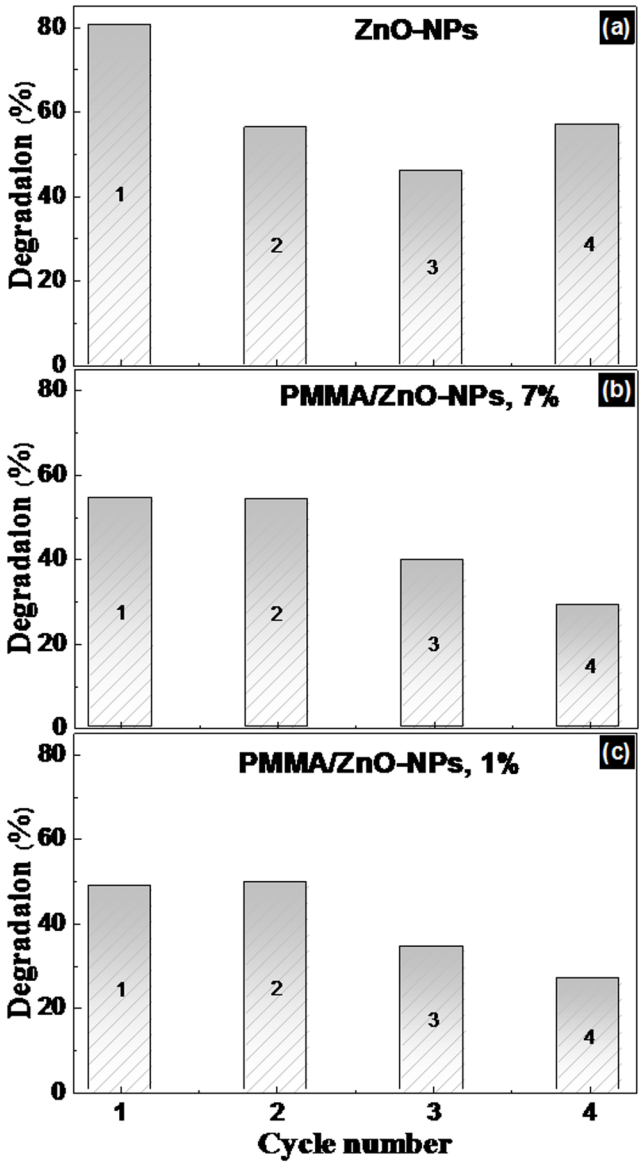

Fig. 11 Reusability of (**a**) ZnO-NPs, (**b**) PMMA/ ZnO-NPs 7%, and (**c**) PMMA/ ZnO-NPs 1% nanocomposites samples for AR dye degradation

ZnO-NPs1% and 7% nanocomposites was determined over four cycles of AR dye degradation, using mass = 70 mg of catalyst at pH = 7, temperature = 22 °C, volume = 25 mL, initial AR concentration = 20 mg/L, and contact time t = 120 min (Fig. 11**(a)**, **(b)**, **(c)**). After each cycle, The samples were washed using a mixture of ethanol and distilled water, filtered, collected, and then dried in an oven for 5 h at 40 °C. The efficiency of degradation decreases from 80.55 to 57.15% for ZnO-NPs, from 54.4 to 29.05% for the content of 7%, and from 48.55 to 26.35% for the content of 1% in PMMA. As shown in Fig. 11, ZnO maintains reasonable activity during the course of the four cycles in degrading AR. The slow gradual decrease in activity is attributed to the loss and photobleaching of ZnO, supporting its potential as a robust and long-term photocatalyst for water pollutant degradation [1, 66]. The decrease in degradation efficiency observed in the third cycle, followed by a slight increase in the fourth cycle for ZnO NPs (Fig. 11), may be attributed to residual dye molecules adsorbed during previous cycles that were not fully removed during the washing step. These residues could have facilitated surface reactivation or contributed to cumulative photocatalytic effects in the subsequent cycle. In contrast, the gradual decrease in efficiency observed for PMMA/ZnO-NPs is likely due to surface fouling, reduced light accessibility, or partial degradation of the polymer matrix, which can hinder the photocatalytic performance over repeated use [51].

Conclusions

This study demonstrates the fabrication of PMMA/ZnO-NPs nanocomposites for potential use in efficient photocatalytic water purification. The main findings underscore their suitability for environmental applications:

i. ZnO nanoparticles exhibit a hexagonal wurtzite structure and are homogeneously distributed within the PMMA matrix.
ii. A strong interaction between ZnO–NPs and PMMA was confirmed by a shift in the C = O stretching vibration. The 3% ZnO–NPs loading, identified as optimal for photodegradation due to its superior dispersion in PMMA matrix, was confirmed by the disappearance of the O–H band and further supported by UV-Vis absorption analysis.
iii. ZnO-NPs and PMMA/ZnO-NPscomposites achieved AR dye photodegradation efficiencies of up to 99% at a concentration of 10 mg/L within 2 h.
iv. Photocatalytic testing on AR dye identifies also an optimal ZnO dosage of 2.8-NPs g/L and 2 g/L for PMMA/ZnO-NPs1% and 7% contents for an ideal irradiation time of 45 min, with degradation efficiency inversely related to dye concentration.
v. PMMA/ZnO-NPs nanocomposites exhibited excellent re-photodegradation performance, making them efficient, cost-effective, and reusable photocatalysts for azo dyes.

Supplementary Information The online version contains supplementary material available at https://doi.org/10.1007/s41779-025-01214-y.

Acknowledgements Authors thank the Algerian Ministry of Higher Education and Scientific Research represented by the Thematic Research Agency in Health and Life Sciences (TRAHLS) for financial support under the National Research Programs (NRP).

Author contributions Hamoudi Belhoul and Smail Terchi: Conceptualization, Methodology, Software Naziha Ladjal and Lamya Meftah: Data curation, Writing- Original draft preparation. Bahri Deghfel and Smail Terchi: Visualization, Investigation. Smail Terchi: Supervision.: Hamoudi Belhoul: Software, Validation.: Abdelhalim Zoukel and Ahmad Azmin Mohamad: Writing- Reviewing and Editing

Funding Not applicable.

Data availability All relevant data are included in the manuscript. The raw data that support the findings of this study are available on request from the corresponding author.

Declarations

Competing interests The authors declare no competing interests.

References

1. Sultana, K.A., Islam, M.T., Silva, J.A., Turley, R.S., Hernandez-Viezcas, J.A., Gardea-Torresdey, J.L., Noveron, J.C.: Sustainable synthesis of zinc oxide nanoparticles for photocatalytic degradation of organic pollutant and generation of hydroxyl radical. J. Mol. Liq. **307**, 112931 (2020)
2. Mohammed, M.I., Khafagy, R.M., Hussien, M.S.A., Sakr, G.B., Ibrahim, M.A., Yahia, I.S., Zahran, H.Y.: Enhancing the structural, optical, electrical, properties and photocatalytic applications of ZnO/PMMA nanocomposite membranes: Towards multifunctional membranes. J. Mater. Sci. Mater. Electron. **33**, 1977–2002 (2022)
3. Kausar, A., Iqbal, M., Javed, A., Aftab, K., Nazli, H., Bhatti, H.N., et al.: Dyes adsorption using clay and modified clay: A review. J. Mol. Liq. **256**, 395–407 (2018)
4. Di Mauro, A., Cantarella, M., Nicotra, G., Pellegrino, G., Gulino, A., Brundo, M.V., Privitera, V., Impellizzeri, G.: Novel synthesis of ZnO/PMMA nanocomposites for photocatalytic applications. Sci. Rep. **7**, 1–12 (2017)
5. Islam, M.T., Dominguez, A., Turley, R.S., Kim, H., Sultana, K.A., Shuvo, M.A.I., Alvarado-Tenorio, B., Montes, M.O., Lin, Y., Gardea-Torresdey, J., Noveron, J.C.: Development of photocatalytic paint based on TiO2 and photopolymer resin for the degradation of organic pollutants in water. Sci. Total Environ. **704** (2020)
6. Zimbone, M., Giuffrida, F., Cantarella, M., Span, V., Sfuncia, G., Lufrano, E., Strano, V., Franz, G., Nicotra, G., Alberti, A., Antonietta, M., Rappazzo, G., Maria, E., Pecoraro, R., Violetta, M., Impellizzeri, G.: ZnO– MoS 2 -PMMA polymeric nanocomposites: A harmless material for water treatment. 36 (2024)
7. Islam, M.T., Dominguez, A., Alvarado-Tenorio, B., Bernal, R.A., Montes, M.O., Noveron, J.C.: Sucrose-Mediated fast synthesis of zinc oxide nanoparticles for the photocatalytic degradation of organic pollutants in water. ACS Omega. **4**, 6560–6572 (2019)
8. Lee, K.M., Lai, C.W., Ngai, K.S., Juan, J.C.: Recent developments of zinc oxide based photocatalyst in water treatment technology: A review. Water Res. **88**, 428–448 (2016)
9. Di Mauro, A., Fragalà, M.E., Privitera, V., Impellizzeri, G.: ZnO for application in photocatalysis: From thin films to nanostructures. Mater. Sci. Semicond. Process. **69**, 44–51 (2017)
10. Gayathri, S., Jayabal, P., Kottaisamy, M., Ramakrishnan, V.: Synthesis of ZnO decorated graphene nanocomposite for enhanced photocatalytic properties. J. Appl. Phys. **115** (2014)
11. Di Mauro, A., Farrugia, C., Abela, S., Refalo, P., Grech, M., Falqui, L., Privitera, V., Impellizzeri, G.: Synthesis of ZnO/PMMA nanocomposite by low-temperature atomic layer deposition for possible photocatalysis applications. Mater. Sci. Semicond. Process. **118**, 105214 (2020)
12. Di Mauro, A., Zimbone, M., Fragalà, M.E., Impellizzeri, G.: Synthesis of ZnO nanofibers by the electrospinning process. Mater. Sci. Semicond. Process. **42**, 98–101 (2016)
13. Maji, P., Choudhary, R.B., Majhi, M.: Structural, electrical and optical properties of silane-modified ZnO reinforced PMMA matrix and its catalytic activities. J. Non Cryst. Solids. **456**, 40–48 (2017)
14. Balen, R., Costa, D., De Lara Andrade, W.V., Piai, J., Muniz, J.F., Companhoni, E.C., Nakamura, M.V., Lima, T.U., Da Cunha Andrade, S.M., Bittencourt, L.H., Hechenleitner, P.R.S., Pineda, A.A.W., Fernandes, E.A.G.: Structural, thermal, optical properties and cytotoxicity of PMMA/ZnO fibers and films: Potential application in tissue engineering. Appl. Surf. Sci. **385**, 257–267 (2016)
15. Singh, A., Mathur, A., Pal, D., Sengupta, A., Singh, R., Chattopadhyay, S.: Near room temperature atomic layer deposition of ZnO thin films on Poly (methyl methacrylate) (PMMA) templates: A study of structure, morphology and photoluminescence of ZnO as an effect of template confinement. Vacuum. **161**, 398–403 (2019)
16. Ocola, L.E., Connolly, A., Gosztola, D.J., Schaller, R.D., Yanguas-Gil, A.: Infiltrated Ainc oxide in poly(methyl methacrylate): An atomic cycle growth study. J. Phys. Chem. C. **121**, 1893–1903 (2017)
17. Jeeju, P. P., Jayalekshmi, S., Chandrasekharan, K., and Sudheesh, P.: Enhanced linear and nonlinear optical properties of thermally stable ZnO/poly (styrene)–poly (methyl methacrylate) nanocomposite films. Thin Solid Films. **531**, 378–384 (2013)
18. Nicolay, A., Lanzutti, A., Poelman, M., Ruelle, B., Fedrizzi, L., Dubois, P., Olivier, M.G.: Elaboration and characterization of a multifunctional silane/ZnO hybrid nanocomposite coating. Appl. Surf. Sci. Elsevier B.V.; (2015)
19. Gao, H., Yorifuji, D., Wakita, J., Jiang, Z.H., Ando, S.: In situ Preparation of nano ZnO/hyperbranched polyimide hybrid film and their optical properties. Polym. (Guildf). **51**, 3173–3180 (2010)
20. Mallakpour, S., Madani, M.: Use of silane coupling agent for surface modification of zinc oxide as inorganic filler and Preparation of poly(amide-imide)/zinc oxide nanocomposite containing phenylalanine moieties. Bull. Mater. Sci. **35**, 333–339 (2012)
21. Tu, Y., Zhou, L., Jin, Y.Z., Gao, C., Ye, Z.Z., Yang, Y.F., Wang, Q.L.: Transparent and flexible thin films of ZnO-polystyrene nanocomposite for UV-shielding applications. J. Mater. Chem. **20**, 1594–1599 (2010)
22. Yang, Z., Peng, H., Wang, W., Liu, T.: Crystallization behavior of poly(ε-caprolactone)/layered double hydroxide nanocomposites. J. Appl. Polym. Sci. **116**, 2658–2667 (2010)
23. Schwartz, V.B., Thétiot, F., Ritz, S., Pütz, S., Choritz, L., Lappas, A., Förch, R., Landfester, K., Jonas, U.: Antibacterial surface coatings from zinc oxide nanoparticles embedded in poly(N-isopropylacrylamide) hydrogel surface layers. Adv. Funct. Mater. **22**, 2376–2386 (2012)
24. Alghamdi, H.M., Rajeh, A.: Study of the photoluminescence, optical, thermal, and electrical parameters of the Cs/PVP blend/zinc oxide nanorods films for energy storage devices. Polym. Test. **124**, 108093 (2023)
25. Yen, L.T., Weng, C.H., Tzeng, J.H., Chen, Y.C., Jacobson, A.R., Lin, Y.T.: Substantial improvement in photocatalysis performance of N-TiO2 immobilized on PMMA: Exemplified by inactivation of Staphylococcus aureus and Escherichia coli. Sep. Purif. Technol. **345**, 127298 (2024)
26. Alvarado-Beltrán, C.G., Almaral-Sánchez, J.L., Quevedo-López, M.A., Ramirez-Bon, R.: Dielectric gate applications of PMMA-TiO2 hybrid films in ZnO-based thin film transistors. Int. J. Electrochem. Sci. **10**, 4068–4082 (2014)

27. Terchi, S., Hamrit, S., Ladjal, N., Bachari, K., Ben Rhaiem, H.: Synthesize of exfoliated poly-methylmethacrylate/organomontmorillonite nanocomposites by in situ polymerization: Structural study, thermal properties and application for removal of Azo dye pollutant. J. Therm. Anal. Calorim. (2024). https://doi.org/10.1007/s10973-023-12810-0
28. El-naggar, A.M., Heiba, Z.K., Kamal, A.M., Bakr Mohamed, M.: Impact of ZnMn2O4/CdS nanocomposite on the structural, optical and dielectric characteristics of PMMA/PEO blend. Results Phys. **56**, 1073235 (2024)
29. Soni, G., Gouttam, N., Joshi, V.: Synthesis and comparisons of optical and gamma radiation shielding properties for ZnO and SiO2 nanoparticles in PMMA nanocomposites thin films. Optik (Stuttg) 259 (2022)
30. Terchi, S., Ladjal, N., Zidelkheir, B., Bachari, K.: ADSORPTION PERFORMANCE OF ANIONIC TEXTILE DYE (NYLOSAN RED N-2RBL) ONTO RAW, SODIC AND FRACTIONATED SODIC INORGANIC CLAY. Mater. Rev. Roum Chim. **65**, 869–884 (2020)
31. Schneider, C.A., Rasband, W.S., Eliceiri, K.W.: NIH image to imageJ: 25 years of image analysis HHS public access. Nat. Methods. **9**, 671–675 (2012)
32. Mohammed, M.I.: Dielectric dispersion and relaxations in (PMMA/PVDF)/ZnO nanocomposites. Polym. Bull. **79**, 2443–2459 (2022)
33. Khaleel, A.K., Abbas, L.K.: Synthesis and characterization of PVDF/PMMA/ZnO hybrid nanocomposite thin films for humidity sensor application. Optik (Stuttg). **272**, 170288 (2023)
34. Hong, R.Y., Qian, J.Z., Cao, J.X.: Synthesis and characterization of PMMA grafted ZnO nanoparticles. Powder Technol. **163**, 160–168 (2006)
35. Poddar, M.K., Sharma, S., Moholkar, V.S.: Investigations in two-step ultrasonic synthesis of PMMA/ZnO nanocomposites by in–situ emulsion polymerization. Polym. (Guildf). **99**, 453–469 (2016)
36. Yousefi, F., Mousavi, S.B., Heris, S.Z., Naghash-Hamed, S.: UV-shielding properties of A cost-effective hybrid PMMA-based thin film coatings using TiO2 and ZnO nanoparticles: A comprehensive evaluation. Sci. Rep. **13**, 1–19 (2023)
37. Khan, M., Chen, M., Wei, C., Tao, J., Huang, N., Qi, Z., Li, L.: Synthesis at the nanoscale of ZnO into poly(methyl methacrylate) and its characterization. Appl. Phys. Mater. Sci. Process. **117**, 1085–1093 (2014)
38. Dey, S., Kar, A.K.: Effect of acceptor concentration in the FRET controlled photoluminescence of PMMA-ZnO nanocomposite for the application of PLED device. Opt. Laser Technol. **136**, 106811 (2021)
39. Youssef, A., El-Nagar, I., El-Torky, A., El-Hakim, A.E.F.A.: Preparation and characterization of PMMA nanocomposites based on ZnO-NPs for antibacterial packaging applications. Proc. World Congr New. Technol. **0**, 1–13 (2019)
40. Verma, G., Singhal, S., Gupta, A.: Nature inspired Ficus Religiosa leaf mesh coated with antibacterial ZnO/PANi@PMMA nanocomposite for separation and water purification. Catal. Commun. **185**, 106806 (2023)
41. Krishna, P.G., Ananthaswamy, P.P., Mutta, N.B., Mariyappa, K.G., Singh, R., Manchegowda, S.H., Dixit, P.S., Shivaprasad, V.: Comparison of antimicrobial and anticancer activity of ZnO nanoparticles prepared using different precursors by hydrothermal synthesis. J. Chem. Pharm. Sci. **10**, 192–197 (2017)
42. Anju Chanu, L., Singh, J., Singh, W.J., Nomita Devi, K.: Effect of operational parameters on the photocatalytic degradation of methylene blue dye solution using manganese doped ZnO nanoparticles. Results Phys. **12**, 1230–1237 (2019)
43. Kaliramna, S., Dhayal, S.S., Kumar, N.: Structural and optical studies of ZnO doped PMMA thin film and its photocatalytic and antibacterial activities. Opt. Mater. (Amst). **133**, 112891 (2022)
44. Ounas, O., Lekhlif, B., Jamal-Eddine, J.: The facile immobilization of ZnO into a polymer surface for photodegradation of organic contaminants. Mater. Today Proc. **30**, 816–822 (2019)
45. Singh, S.P., Sharma, S.K., Kim, D.Y.: Carrier mechanism of ZnO nanoparticles-embedded PMMA nanocomposite organic bistable memory device. Solid State Sci. **99**, 106046 (2020)
46. Kango, S., Kalia, S., Celli, A., Njuguna, J., Habibi, Y., Kumar, R.: Surface modification of inorganic nanoparticles for development of organic-inorganic nanocomposites - A review. Prog Polym. Sci. **38**, 1232–1261 (2013)
47. Hammani, S., Barhoum, A., Bechelany, M.: Fabrication of PMMA/ZnO nanocomposite: Effect of high nanoparticles loading on the optical and thermal properties. J. Mater. Sci. **53**, 1911–1921 (2018)
48. Amari, R., Guellil, A., Terchi, S., Deghfel, B., Zoukel, A., Allali, D., Benrezgua, E., Boukhari, A., Mohamad, A.A.: Coprecipitation synthesis of transition metal (Al, Mn, Cu, Ag) doped zinc oxide nanopowders: Characterization, photocatalytic test, and comparison study. J. Aust Ceram. Soc. (2023). https://doi.org/10.1007/s41779-023-00969-6
49. Cui, C.W., Yang, C., Bao, J., Huang, X.J., Zeng, X.F., Chen, J.F.: Monodispersed ZnO Nanoparticle-Poly(methyl methacrylate) composites with visible transparency for ultraviolet shielding applications. ACS Appl. Nano Mater. (2020)
50. Paulista, A.P.F., Barbosa, F.F., Júnior, M.A., do, N., Cavalcanti, W.E.C., Soares, J.O., Morales, M., Pergher, S.B.C., Braga, T.P.: Photocatalytic degradation of the remazol red ultra RGB dye using SrFe12O19-Fe3O4 magnetic oxides dispersed in silica: Effect of reduction temperature. Desalin. Water Treat. **320** (2024)
51. Hokonya, N., Mahamadi, C., Mukaratirwa-Muchanyereyi, N., Gutu, T., Zvinowanda, C.: Green synthesis of P–ZrO2CeO2ZnO nanoparticles using leaf extracts of Flacourtia indica and their application for the photocatalytic degradation of a model toxic dye, congo red. Heliyon. **8**, 10277 (2022)
52. Ullah, S., Shahid, W., Shahid, S., Khan, M.I., Ansar, N., Khizar, M., Ali, S., Choi, R., Almutairi, J., Alreshidi, B.S.A.: Advancing photocatalysis: Innovative approaches using novel V2O5/ZnO nanocomposites for efficient photocatalytic degradation of Tubantin red. J. Saudi Chem. Soc. **27**, 101766 (2023)
53. Rani, M., Shanker, U.: Sun-light driven rapid photocatalytic degradation of methylene blue by poly(methyl methacrylate)/metal oxide nanocomposites. Colloids Surf. Physicochem Eng. Asp. **559**, 136–147 (2018)
54. Sekaran, C., Dhandapani, B., Alagesan, T., Balaji, G.: Enhanced photocatalytic degradation kinetics of azo-dyes by novel Ni2+and Ag2+doped ZnO nanocatalysts. Appl. Surf. Sci. Adv. **12**, 0–5 (2022)
55. Hameed, B.H., Akpan, U.G., Wee, K.P.: Photocatalytic degradation of acid red 1 dye using ZnO catalyst in the presence and absence of silver. Desalin. Water Treat. **27**, 204–209 (2011)
56. Bhamare, V.S., Kulkarni, R.M.: Photocatalytic degradation of Zidovudine by 0.8% ruthenium doped titanium dioxide nanoparticles during water treatment: Synthesis, characterisation, kinetics and mechanism. Desalin. Water Treat. **182**, 288–298 (2020)
57. Shahmoradi, B., Pordel, M.A., Pirsaheb, M., Maleki, A., Kohzadi, S., Gong, Y., Pawar, R.R., Lee, S.M., Shivaraju, H.P., McKay, G.: Synthesis and characterization of barium-doped TiO2 nanocrystals for photocatalytic degradation of acid red 18 under solar irradiation. Desalin. Water Treat. **88**, 200–206 (2017)
58. Pishrafti, H., Kamani, H., Mansouri, N., Hassani, A.H., Ahmadpanahi, H.: Photocatalytic removal of the erythromycin antibiotic using Fe-doped TiO2 @Fe3 O4 magnetic nanoparticles:

Investigation of effective parameters, process kinetics and degradation end products. Desalin. Water Treat. **262**, 323–337 (2022)
59. Brishti, R.S., Ahsan Habib, M., Ara, M.H., Rezaul Karim, K.M., Islam, K., Naime, M., Rumon, J.H., Rayhan, M.M., Khan, M.A.: Green synthesis of ZnO NPs using aqueous extract of Epipremnum aureum leave: Photocatalytic degradation of congo red. Results Chem. **7**, 101441 (2024)
60. Hemanathan, G., Karthikeyan, S., Kathirvel, R.: Comparative study on solar photocatalytic degradation of Naproxen using nitrogen doped ZnO and nitrogen doped TiO2: Kinetics and intermediates analysis. Desalin. Water Treat. **320**, 100675 (2024)
61. Zhu, J., Shao, C., Li, X., Han, C., Yang, S., Ma, J., et al.: Immobilization of ZnO/polyaniline heterojunction on electrospun polyacrylonitrile nanofibers and enhanced photocatalytic activity. Mater. Chem. Phys. **214**, 507–515 (2018)
62. Altin, I., Sökmen, M.: Buoyant photocatalyst based on ZnO immobilized on polystyrene beads for pollutants treatment. Clean. - Soil. Air Water. **43**, 1025–1030 (2015)
63. Rezeki, Y.A., Setyaningsih, L.D., Budi, H.S., Angel, J., Fahroji, M., Amalia, R., Arrosyid, B.H., Handika, G., Saputro, K.E., Noviyanto, A., Zulfi, A.: Fabrication of nanofiber membranes from Waste-Expanded polystyrene (EPS) combined with zinc oxide nanoparticles (ZnO NPs) and its photocatalytic activity. Trends Sci. **21**, 1–12 (2024)
64. Mulatu Mamo, G., Yadeta Ejeta, S.: Copper Oxide-Nickel oxide nanocomposites synthesized via Allium cepa Peel extract for photocatalytic degradation of methylene blue. Results Chem. **11**, 101801 (2024)
65. Rianjanu, A., Marpaung, K.D.P., Siburian, C., Muhtar, S.A., Khamidy, N.I., Widakdo, J., Yulianto, N., Aflaha, R., Triyana, K., Taher, T.: Enhancement of photocatalytic activity of CeO2 nanorods through lanthanum doping (La–CeO2) for the degradation of congo red dyes. Results Eng. **23**, 102748 (2024)
66. Montazerghaem, L., Keramatifarhodbonab, M., Naeimi, A.: Photocatalytic degradation of acid blue 74 by Co: WO3 nanoparticles: Kinetics and response surface methodology studies. Heliyon. **10**, 24789 (2024)